Evolution of Stationary Crossflow Vortices in Boundary Layers on Swept Wings

R. D. Joslin

Reprinted from

AIAA Journal

Volume 33, Number 7, Pages 1279–1285

AIAA

A publication of the
American Institute of Aeronautics and Astronautics, Inc.
370 L'Enfant Promenade, SW
Washington, DC 20024-2518

AIAA JOURNAL
Vol. 33, No. 7, July 1995

Evolution of Stationary Crossflow Vortices in Boundary Layers on Swept Wings

Ronald D. Joslin*
NASA Langley Research Center, Hampton, Virginia 23681-0001

The spatial evolution of crossflow–vortex disturbances in a laminar boundary layer on a swept wing is computed by the direct numerical simulation of the incompressible Navier–Stokes equations. A wall-normal velocity distribution of steady suction and blowing at the wing surface is used to generate a strip of equally spaced and periodic disturbances along the span. Three simulations are conducted to study the effect of initial amplitude on both the disturbance evolution and to provide a database for transition-onset prediction methods. As an example application, a theory for a transition model is compared with the direct numerical simulations data. In each simulation, the vortex disturbances first enter a chordwise region that can be described as linear growth; then, the individual disturbances coalesce downsteam and either superpose linearly or interact nonlinearly with adjacent modes; finally, the crossflow vortices enter a region that contains strong nonlinear interactions sufficient to generate inflectional velocity profiles. As the initial amplitude of the disturbance increases (roughness size increases), the length of the evolution to breakdown decreases. In the example application, the three simulations collapse onto a single curve, which is an intermittency correlation for a transition model.

I. Introduction

BECAUSE of fierce competition and rising operational costs, the aircraft industry must utilize advanced technology in the design of the next generation of aircraft, for example, the reduction of external viscous drag (and fuel expenditures) by both natural laminar flow control and the laminar flow control of the three-dimensional boundary-layer flow on the wings of the aircraft. The fuel savings translates directly into reduced operating costs in terms of millions of dollars over the life of a single aircraft.[1] Improvements in wing designs[2] and the implementation of devices such as suction for laminar flow control[3] and Gaster's bump[4] successfully reduce aircraft drag. These technological advances are successful because they are based (in part) on a fundamental understanding of three-dimensional boundary-layer flow physics. As the mechanisms of transition are better understood, the transition process can be more easily predicted, modeled, and controlled. The present paper is devoted to extending the knowledge of transition in a swept-wing flow to aid future transition models and transition-onset prediction methods.

Earlier experiments by Arnal et al.,[5] Poll,[6] Bippes and Nitschke-Kowsky,[7] Müller and Bippes,[8] Dagenhart et al.,[9] and Dagenhart and Saric[10] have shown that both stationary and traveling crossflow vortices are present within the three-dimensional boundary layers of swept-wing flows. These instabilities are spawned from inflections in the mean velocity profile and are prevalent in regions of favorable pressure gradients (i.e., near the leading edge). Tollmien–Schlichting traveling waves are suppressed in these regions. High levels of freestream turbulence lead to dominant traveling crossflow vortices; stationary disturbances are dominant in a quiet freestream (flight conditions). In contrast to experimental results, linear theory[11,12] predicts that traveling crossflow disturbances have large growth rates and, therefore, dominate transition.

Choudhari and Streett[13] and Crouch[14] have shown with receptivity theory that freestream noise, coupled with roughness elements on the wing surface, generates dominant stationary disturbances with amplitudes much larger than those for traveling modes. Although the growth rates associated with traveling crossflow modes are larger than those of stationary crossflow vortices, the initial large amplitude of the stationary mode, in comparison with that of traveling modes, causes the stationary mode to dominate the instability process if the freestream is relatively quiet.

Based on the receptivity results, Joslin and Streett[15] used direct numerical simulations (DNS) to identify three distinct stages in the stationary crossflow breakdown process in swept-wedge flow. They found that disturbances undergo stages of linear growth followed by a coalescence of vortex packets. If the disturbance amplitudes are sufficiently small at coalescence, then this coalescent stage can be described as a linear superposition of disturbances. Finally, downstream of coalescence, nonlinear interactions and vortex rollover characterize the later stage of breakdown. In the later stage, inflectional velocity profiles were observed; this observation is consistent with the experimental results of Dagenhart and Saric[10] and the computational results of Lin and Reed[16] and Fuciarelli and Reed.[17]

Related to the previous study by Joslin and Streett,[15] here two additional simulations are conducted to aid future amplitude-based transition-prediction models (e.g., parabolized stability equation theory) and to document the effects of initial amplitudes on disturbance development. A transition model is used as an example application of the DNS data.

II. Mathematical Model

To solve the problem numerically, the instantaneous velocities $\tilde{\boldsymbol{u}} = (\tilde{u}, \tilde{v}, \tilde{w})$ and the pressure $\tilde{p}$ are decomposed into base and disturbance components. The base flow is given by velocities $\boldsymbol{U} = (U, V, W)$ and the pressure P; the disturbance is given by velocities $\boldsymbol{u} = (u, v, w)$ and the pressure p. The velocities correspond to the coordinate system $\boldsymbol{x} = (x, y, z)$, where x is the chordwise direction, y is the wall-normal direction, and z is the spanwise direction. A sketch of the swept-wing problem is shown in Fig. 1. Note that the wing-sweep direction corresponds to the positive z direction and the direction of positive spanwise velocity. The computational domain is identified by region 2 of the figure. (Region 1 of the figure corresponds to the computational domain for the study of the attachment-line region.)

The base flow for the swept wedge is described by the Falkner–Skan–Cooke (FSC) similarity profiles.[18,19] To generate the velocity field, an analytical pressure gradient is imposed. This pressure matches the experimental results of Müller and Bippes[8] for their swept-wedge model.

Received Aug. 10, 1994; revision received Jan. 23, 1995; accepted for publication Jan. 24, 1995.

*Research Engineer, Fluid Mechanics and Acoustics Division. Member AIAA.

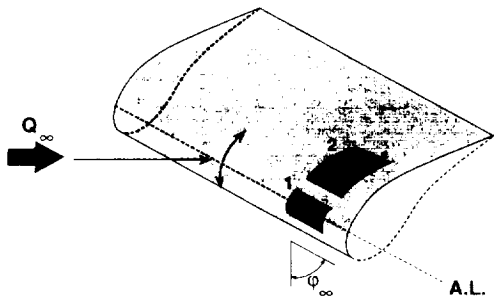

Fig. 1 Sketch of swept-wing 1) attachment-line region and 2) laminar-to-turbulent transition region.

For the disturbance portion of Eq. (1), the three-dimensional, incompressible Navier–Stokes equations are solved in disturbance form. These equations are given by

$$\boldsymbol{u}_t + (\boldsymbol{u}\cdot\nabla)\boldsymbol{u} + (\boldsymbol{U}\cdot\nabla)\boldsymbol{u} + (\boldsymbol{u}\cdot\nabla)\boldsymbol{U} = -\nabla p + (1/Re)\nabla^2\boldsymbol{u} \quad (1)$$

with the continuity equation

$$\nabla\cdot\boldsymbol{u} = 0 \quad (2)$$

and boundary conditions

$$\boldsymbol{u} = 0 \quad \text{at} \quad y = 0 \quad \text{and} \quad \boldsymbol{u} \to 0 \quad \text{as} \quad y \to \infty \quad (3)$$

The Reynolds number $Re = Q_R\delta/\nu$ is based on the boundary-layer thickness in the xy plane defined as $\delta = \sqrt{\nu x_c/U_0}$ (where x_c is the chordwise coordinate normalized by the chord length) and the local edge velocity $Q_R = Q_0$ at the computational inflow.

III. Numerical Method of Solution

In this section, the numerical techniques required for the simulation and the disturbance forcing are briefly discussed. For a detailed description of the spatial DNS approach used for this study, refer to Joslin et al.[20,21]

The spatial discretization entails a Chebyshev collocation grid in the wall-normal direction, fourth-order finite differences for the pressure equation, sixth-order compact differences for the momentum equations in the streamwise direction, and a Fourier series in the spanwise direction on a staggered grid.[21] For time marching, a time-splitting procedure is used with implicit Crank–Nicolson differencing for normal diffusion terms and an explicit three-stage Runge–Kutta method.[22] The influence-matrix technique is employed to solve the resulting pressure equation (Helmholtz–Neumann problem).[23,24] Disturbances are introduced into the boundary layer by suction and blowing techniques. At the inflow boundary, the mean base flow is forced, and, at the outflow, the buffer-domain technique of Streett and Macaraeg[25] is used.

In this study, the vortex packets are forcibly imposed into the boundary layer by steady suction and blowing through the wedge surface in the same manner as described by Joslin and Streett.[5] Suction and blowing techniques may be used because, as demonstrated by Kachanov and Tararykin,[26] the results from suction and blowing and roughness-element disturbance generators correlate well and lead to disturbances that graphically coincide.

IV. Computational Test Cases

For the simulations, no surface imperfections, particulates, weather-condition effects, noise, or spanwise inhomogeneities exist. Surface curvature is neglected to simplify the numerics and because the simulation is conducted on a chordwise region of the wing that corresponds to a relatively flat portion of a laminar flow airfoil.[9] The base flow and most of the parameters used in the initial study by Joslin and Streett[15] are used here to enlarge the database and enhance the understanding of the transition process on swept wings.

The first simulation (SIM-I) is the case of Joslin and Streett.[15] This simulation has a grid of 901 streamwise, 61 wall-normal, and 32 spanwise grid points. The far-field boundary is located 50δ from the wedge, the streamwise distance is 857δ from the inflow, and the spanwise distance in 108δ. For the time marching, a time-step size of 0.2 is chosen for the three-stage Runge–Kutta method. For all simulations, crossflow–vortex packets are generated through a periodic strip of steady suction and blowing holes that are equally spaced on the wing surface, and the shape of the wall-normal velocity profiles at the wall have a half-period sine wave in the chordwise direction and a full-period sine wave in the spanwise direction. This mode of disturbance generation would correspond to an isolated roughness element within the computational domain. Stationary crossflow–vortex packets are generated by steady suction and blowing with a wall-normal velocity component at the wall with an amplitude of $v_w = 1 \times 10^{-5}$. The holes for SIM-I have a chordwise length of 8.572δ and a spanwise length of 16.875δ.

The second simulation (SIM-II) has a grid of 901 streamwise, 81 wall-normal, and 48 spanwise grid points. The far-field boundary is located 50δ from the wedge, the streamwise distance is 550δ, and the spanwise distance is 108δ. A time-step size of 0.2 is chosen for time marching. Suction and blowing with a wall-normal velocity amplitude of $v_w = 1 \times 10^{-4}$ is used to generate the stationary crossflow vortices. The holes for SIM-II have a chordwise length of 8.5δ and a spanwise length of 36δ. These holes are aligned side by side in the spanwise direction.

The final simulation (SIM-II) has a grid of 721 streamwise, 81 wall-normal, and 64 spanwise grid points. The far-field boundary is located 50δ from the wedge, the streamwise distance is 440δ, and the spanwise distance is 108δ. A time-step size of 0.2 is chosen for time marching. Stationary crossflow–vortex packets are generated with steady suction and blowing with a wall-normal velocity component at the wall with an amplitude $v_w = 1 \times 10^{-3}$. The holes for SIM-III have a chordwise length of 5.5δ and a spanwise length of 36δ. These holes are aligned side by side in the spanwise direction.

A grid refinement study for the DNS code was described by Joslin et al.[20] Further, the parameters used in SIM-II and SIM-III are based on the experience gained by the Joslin and Streett[15] study. Evidence to support sufficient resolution is used for each case is confirmed in the example application presented in Sec. VI, where the nonlinear portion of the solutions collapse onto a single curve. The time-step size is much smaller than the Courant–Fredricks–Lewy (CFL) limit; the reduced size was selected to ensure that no transient or time-dependent numerical noise was introduced in these simulations.

V. Stages of Disturbance Evolution

Distinct stages of disturbance evolution were previously observed and described in some detail by Joslin and Streett.[15] They observed that the initial growth of individual disturbance packets occurred in isolation from adjacent packets. The individual packets coalesced at a chordwise location downstream, depending on the distance between the suction holes, the directions of the disturbance evolution, and the spreading rate. When the vortex packets reach sufficiently large amplitudes in the later stages of transition, the disturbance field was dominated by nonlinear interactions and vortex rollover. These stages are sketched in Fig. 2, where spanwise slices (planes) of chordwise velocity contours viewed from the trailing edge toward the leading edge are shown. (The wing tip is to the left, and the wing root is to the right.) For each simulation, the contour results show that immediately downstream of the disturbance initialization point a distinct vortex packet evolves that is isolated from nearby disturbances. As the disturbance evolves and spreads, additional vortices fill the span as a result of the adjacent vortex superposition. This superposition process leads to apparent rapid increases in the disturbance amplitudes and phase adjustments. In the later, nonlinear stage of breakdown, the contours indicate that low-speed fluid is dragged out and over the high-speed fluid, which is drawn toward the surface. Dagenhart and Saric[10] observed this same phenomenon in their experimental results.

The breakdown sequence of SIM-I may be typical for isolated roughness elements, where initial energy resides in many instability modes, but the evolution sequence can be more generalized by the following description. Instead of describing the first stage as a region of isolated growth (which is specific to an isolated roughness), the initial growth stage should be described as a "linear" or exponen-

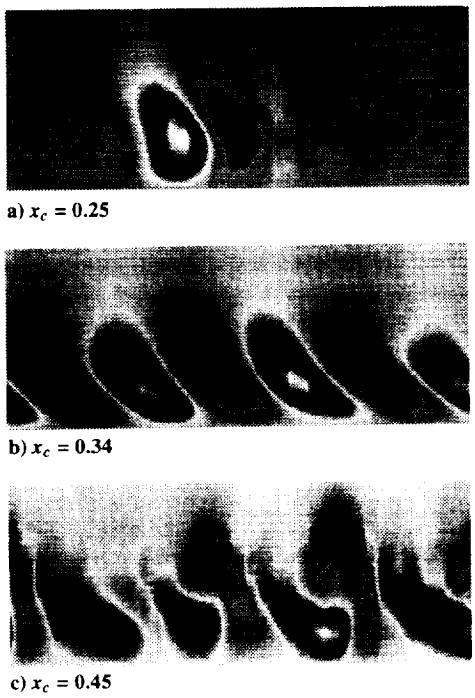

Fig. 2 Spanwise planes of disturbance velocity u contours at chordwise locations for swept-wedge flow of SIM-I.

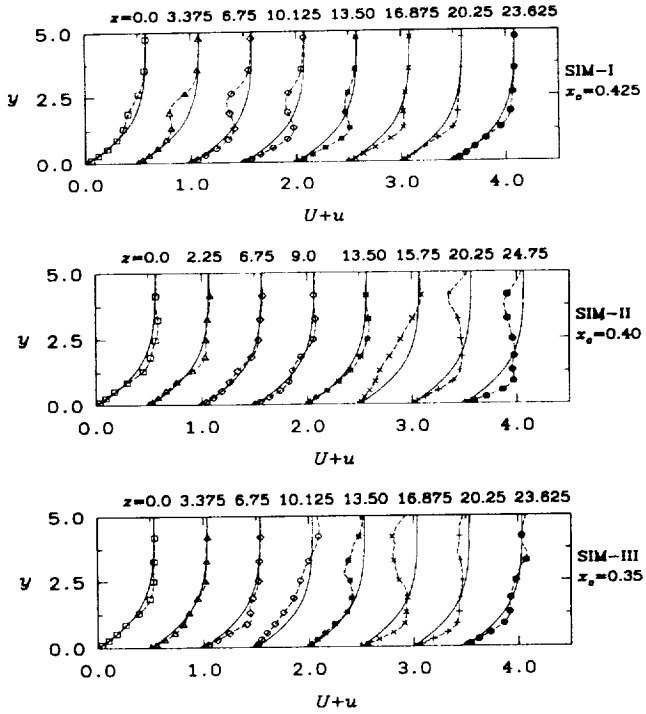

Fig. 3 Chordwise (base + disturbance) velocity profiles at various chordwise and spanwise locations for swept-wedge flow.

tial growth stage. In both SIM-II and SIM-III, the initial amplitude levels of the disturbances are much larger than SIM-I, and the disturbance initiation process imitates distributed roughness, where initial energy resides in a single dominant mode; yet, all of the simulations have this linear growth stage. The second stage can be generically described as coalescence, although, unlike SIM-I which is linear superposition, the process may be nonlinear in SIM-II and/or SIM-III because of the much larger disturbance amplitudes. The final stage can be typically described as a nonlinear interaction stage because all of the simulations have very large amplitudes in this region. Further discussion of the stages of evolution are reserved for Sec. VII.

In this nonlinear interaction region, inflectional velocity profiles are observed in all of the simulations. Figure 3 shows the instantaneous chordwise velocity profiles ($U + u$) for each simulation at a chordwise station that corresponds to the nonlinear vortex rollover stage; the various profiles at each station correspond to adjacent spanwise locations. Across the span, the flow is accelerated in regions near the wedge surface and is retarded in other areas out in the boundary layer. The characteristic inflectional profiles have been observed in experiments by Müller and Bippes,[8] Dagenhart et al.,[9] and Dagenhart and Saric[10] and in computations by Lin and Reed,[16] Fuciarelli and Reed,[17] and Joslin and Streett.[15] Dagenhart and Saric[10] noted that the appearance of inflectional profiles was rapidly followed by the appearance of a high-frequency instability and, subsequently, by transition. The theoretical studies of Kohama et al.,[27] Reed and Fuciarelli,[28] and Balachandar et al.[29] indicated that this high-frequency instability in the experiments is reminiscent of secondary instabilities, which spawn from these inflectional velocity profiles.

VI. Transition Prediction

The transition region is usually defined as the spatial region between flow regimes which are statistically characterized by laminar flow (although unstable disturbances may be imbedded and evolving in the laminar flow) and fully developed turbulent flow. One conventional measure of transition onset is a deviation, or rise, in the skin-friction coefficient c_f from the laminar value and heading toward the turbulent value. Thus, the chordwise point of this often rapid rise in c_f could be defined as the transition point. For the three simulations, instantaneous skin-friction coefficients which chord location are shown in Fig. 4 at a spanwise location corresponding to $z = 0$. (The location $z = 0$ is reminiscent of all spanwise locations.) These local values correspond to skin-friction oscillations about the base (laminar) flow. The velocity profiles in Fig. 3 aid in the explanation of these oscillations. A cross-sectional slice of the crossflow disturbances indicates regions of accelerated and retarded flow. The accelerated regions exhibit a rise in the skin-friction coefficient; areas of retarded flow show a decrease in the skin friction. A comparison of the results for the different simulations clearly show that as the initial amplitude of the disturbances increases the skin-friction distribution becomes less organized.

The local measure of the skin friction is not usually used for determining the onset of transition; rather, an average skin-friction display is conventional. The spanwise average skin friction with chord location is shown in Fig. 5 for the three simulations. As ex-

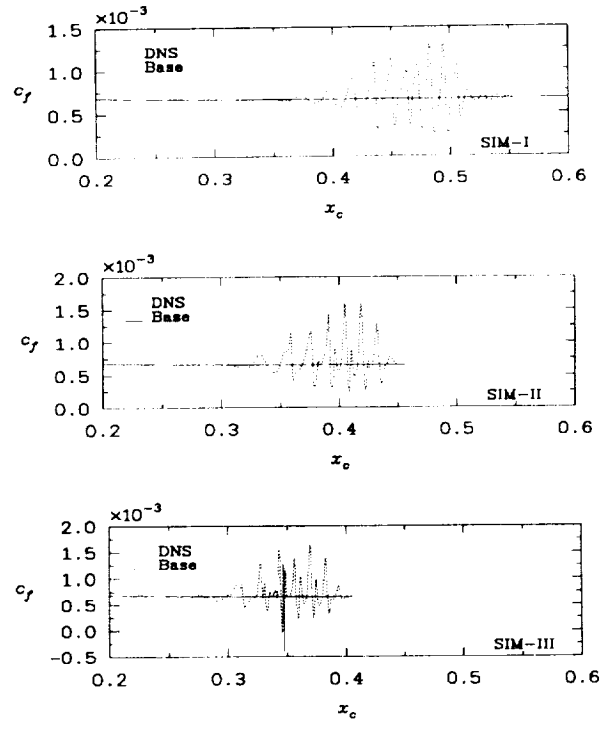

Fig. 4 Instantaneous skin-friction coefficients at $z = 0$.

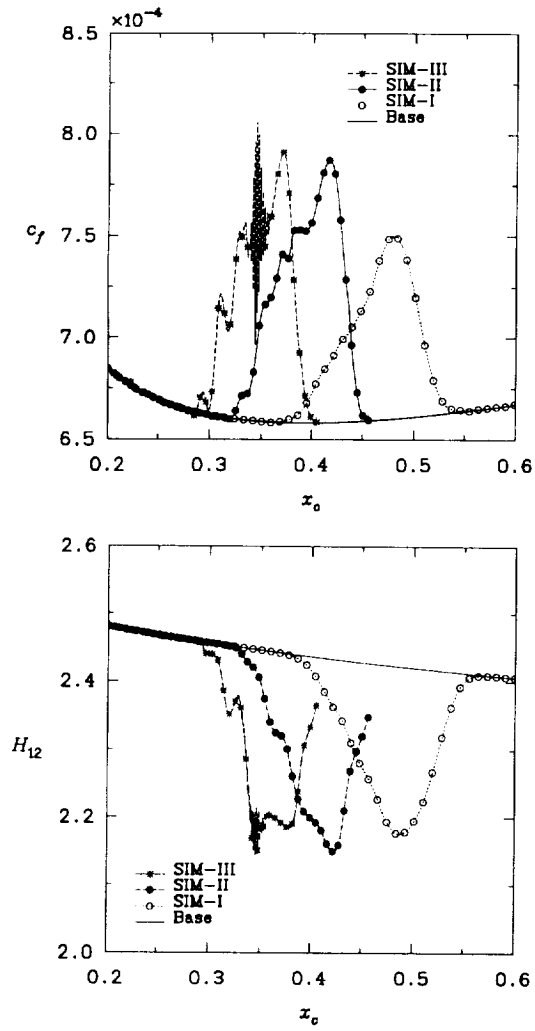

Fig. 5 Average skin-friction coefficients c_f and shape factors H_{12}.

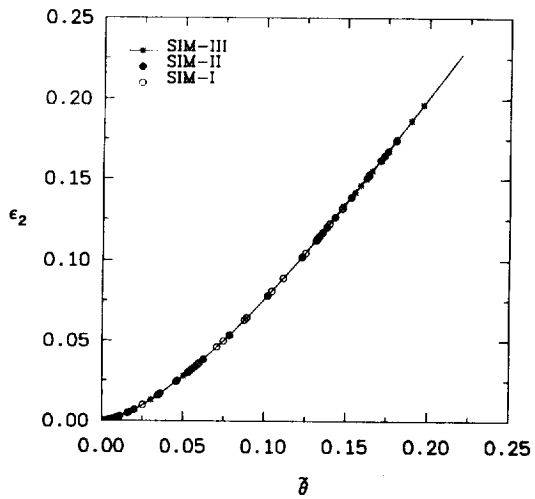

Fig. 6 Weighting coefficients ϵ_2 and momentum factor $\tilde{\theta}$.

pected, the disturbance initiated with the smallest amplitude evolves farthest along the chord prior to transition. The intermittent skin-friction behavior of the larger amplitude cases is pronounced. Another indication of the onset of transition is the chordwise shape factor (the displacement thickness divided by the momentum thickness). Comparisons of the simulation results are also shown in Fig. 5. Both the skin friction and the shape factor show the onset of transition for SIM-I at approximately $x_c \simeq 0.40$, for SIM-II at $x_c \simeq 0.33$, and for SIM-III at $x_c \simeq 0.28$. For all of these simulations, the very early stage of the onset of transition is computed. If the simulations were continued, much greater grid resolution would be required and unsteady modes would need to be included in the disturbance generation process. Additionally, the results would show a continued rise in skin friction and decrease in shape factor. However, the results of the simulation shown in Figs. 4 and 5 apparently indicate that peak values are reached. This occurs because the simulations were discontinued before all transient effects could pass out of the computational domain.

In an experimental and theoretical study, Arnal et al.[5] compared various parameters from their experiments with results from calculations. The agreement was good, although only a few experimental data points were shown. For the calculations, they represented quantities in the transition region by a conventional intermittency relationship between laminar and turbulent quantities. This intermittency relationship is

$$A = (1 - \epsilon_2)A_l + \epsilon_2 A_t \tag{4}$$

$$1/B = (1 - \epsilon_2)(a/B_l) + \epsilon_2(1/B_t) \tag{5}$$

where A is the shape factor H_{12}, the skin friction c_f, and the entrainment coefficients C_e, and B is the momentum thickness θ; the subscripts l and t refer to laminar and turbulent values, respectively; ϵ_2 in an appropriate weighting factor. The weighting factor is defined as a function of the momentum thickness θ divided by the value at transition (θ_T) and ranged from 0 for laminar flow to 1 for turbulent flow. Here, the weighting factor associated with the global equations is tested against the simulation data to determine if the concept might be useful for inclusion in theories of transition modeling.

The weight factor ϵ_2 was defined by Arnal et al.[5] as

$$\epsilon_2 = 1 - \exp[-2.5\tilde{\theta}^{1.5}] \tag{6}$$

where $\tilde{\theta} = \theta/\theta_T - 1$. The weights obtained by substituting the momentum thicknesses from each simulation into Eq. (6) are shown in Fig. 6. Clearly, the three simulations collapse onto the single curve for the early stages of transition. Based on the definition of ϵ_2, the results in Fig. 6 indicate that the present simulations have made it approximately 20% of the way through transition. In order to fully rely on such a weighting of laminar-to-turbulent (transition) properties, the simulation results would need to be extend from laminar to completely turbulent flow, which is beyond the scope of this paper.

Note that the description of the transition region given in Eqs. (4–6) require some a priori knowledge of transition and turbulent values. The present DNS data is offered also to validate future transition-onset prediction methods.

VII. Spectral Analysis

Because the present DNS code uses a Fourier series as the spanwise representation of the disturbance, spanwise spectra can readily be obtained by transforming the physical results to wave number space. Figure 7 shows the maximum amplitude of the chordwise velocity of the decomposed dominant spanwise mode. The simulation cases followed similar evolution patterns (discussed in Sec. V) and saturate at nearly the same amplitude of approximately 10% of the edge velocity.

Given the small initial disturbance amplitude and the explanation of the superposition process of adjacent vortex packets,[15] the sudden and nonuniform increase in amplitude evident in SIM-I can be explained by a linear process. In SIM-III, however, the merging process may not be attributed to superposition; it may be nonlinear because of the much larger disturbance amplitudes involved. To resolve this uncertainty, Fig. 8 shows the terms in the Navier–Stokes equation for the dominant mode.

Figure 8 shows both the dominant mode and the mean-flow distortion of the chordwise velocity, as well as a linear and nonlinear convection terms. The first visible evidence of the coalescence appears in the dominant spectral component. As described by Joslin and Streett,[15] the merging of vortex packets causes not only changes in amplitudes but a region of wave-angle adjustment. By comparing

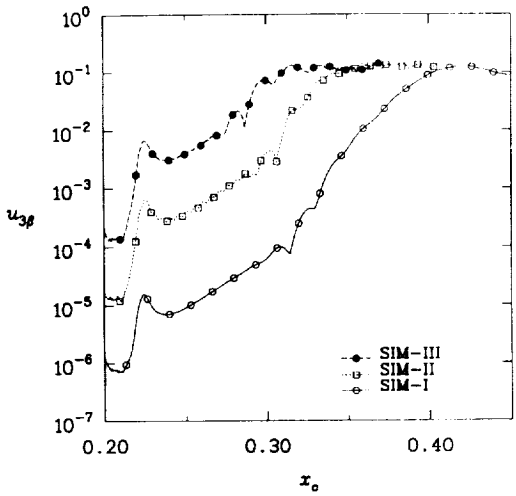

Fig. 7 Amplitude of disturbance mode with chordwise location for swept-wedge flow.

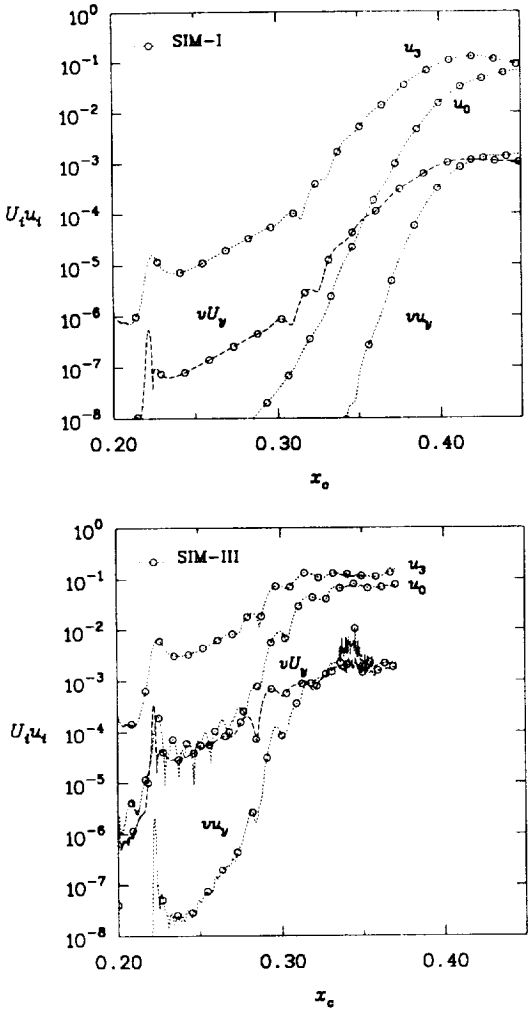

Fig. 8 Amplitude of disturbance mode, mean-flow distortion, and linear and nonlinear convection terms with chordwise location for swept-wedge flow.

the maxima for the spectrum of the nonlinear terms in the Navier–Stokes equations with the dominant velocity modes of SIM-I in Fig. 8, we find that the nonlinear terms are four orders of magnitude smaller than the linear velocity component terms and two orders of magnitude smaller than the linear convection terms in this coalescent region. Additionally, the distortion to the mean flow due to nonlinear interactions does not become significant in comparison

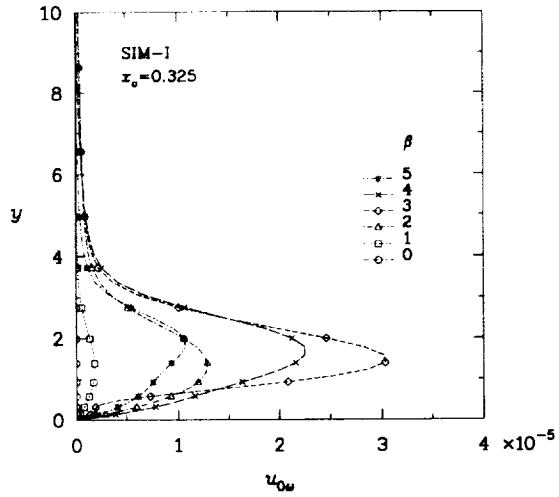

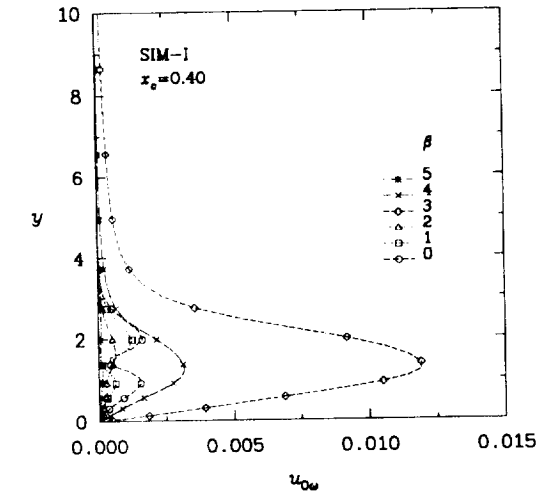

Fig. 9 Profiles of crossflow disturbance mode and spanwise harmonics.

with the disturbance velocity until $x_c \simeq 0.40$, where transition was shown to occur in Fig. 5. For SIM-III, however, the larger initial amplitude causes a more severe distortion to the mean flow, and the so-called coalescence becomes a nonlinear interaction phase in this simulation. At this chordwise location, the amplitude of the nonlinear terms rapidly increase and become comparable to those of the linear convection terms, and the amplitude of mean-flow distortion becomes comparable to that of the disturbance velocity. This region of rapidly rising amplitudes is the location at which transition occurs ($x_c \simeq 0.28$ in Fig. 5).

Finally, Figs. 9, 10, and 11 show the stationary crossflow disturbance profiles before the coalescent stage and at the location of the onset of transition (i.e., the point at which c_f rises and H declines) for SIM-I, SIM-II, and SIM-III, respectively. Because an isolated roughness element was used in SIM-I, a crossflow–vortex packet was generated, which causes multiple modes to grow (see the first portion of Fig. 9). In SIM-II and SIM-III, a continuous distribution was used to generate the single crossflow mode shown in Figs. 10 and 11. Near the transition onset location, the distortion to the mean flow becomes significant in all simulations. This distortion is accomplished primarily because a single dominant mode has gained sufficient amplitude (or energy) to permit nonlinear interactions; this phenomenon is evident in the second portion of Figs. 9–11. Recall that in this region the low-speed fluid near the wall is dragged over the high-speed fluid and the mean velocity profiles are highly inflectional (Fig. 3), which enhances the instability of unsteady modes. The transition process could not continue without the introduction of unsteady modes because the stationary crossflow vortex saturates, as shown in Fig. 7. These results demonstrate that a linear growth stage occurs whether or not a vortex packet is generated and regardless of the individual vortex modes and the initial amplitudes

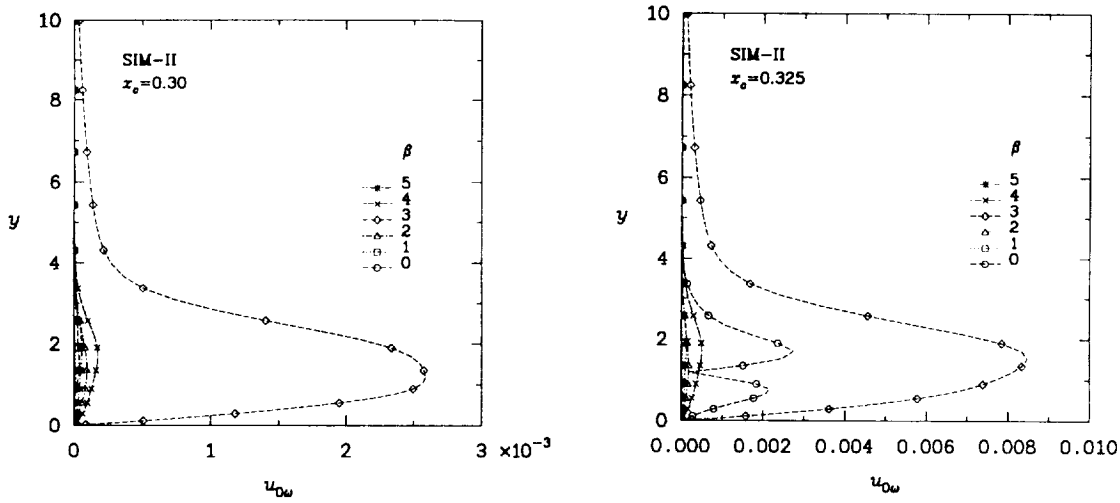

Fig. 10 Profiles of crossflow disturbance mode and spanwise harmonics.

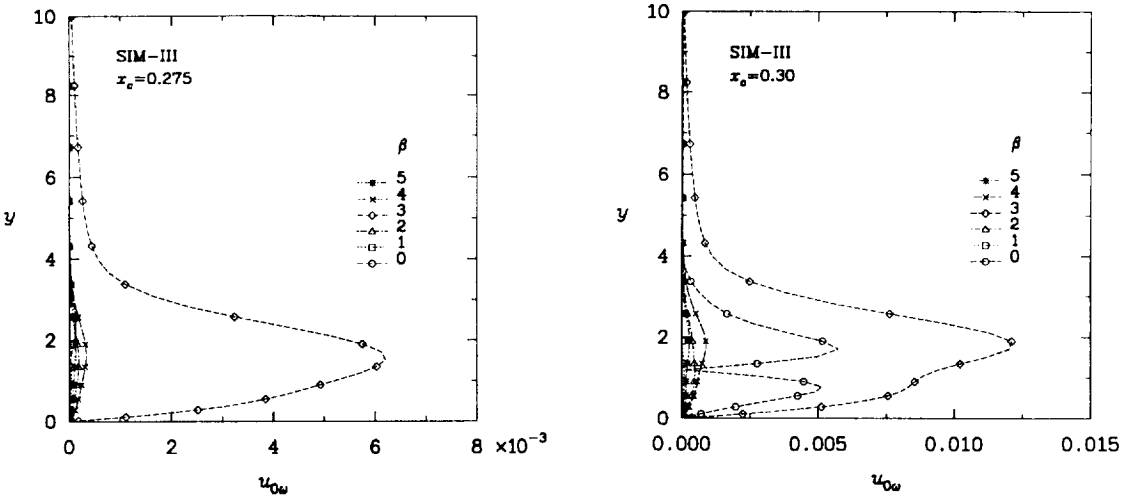

Fig. 11 Profiles of crossflow disturbance mode and spanwise harmonics.

of the modes; however, the length of this linear region is a function of the initial disturbance amplitudes. Also, the merging (or coalescent) process can be either linear superposition or nonlinear, depending on the initial amplitudes of the disturbances.

VIII. Concluding Remarks

The spatial evolution of crossflow–vortex disturbances in a laminar boundary layer on a swept wing was computed by direct numerical simulation of the incompressible Navier–Stokes equations. Three distinct stages of disturbance evolution were observed in all simulations; these results agree with the previous study by Joslin and Streett.[15] A disturbance that is ingested into the flow will eventually interact nonlinearly and lead to inflectional profiles; these inflectional profiles are observed experimentally just prior to the laminar-to-turbulent transition location. The characteristic inflectional profiles have been observed in experiments by Müller and Bippes,[8] Dagenhart et al.,[9] and Dagenhart and Saric[10] and in computations by Lin and Reed,[16] Fuciarelli and Reed,[17] and Joslin and Streett.[15]

Skin-friction and shape-factor comparisons were used to indicate the onset of transition. As expected, the transition-onset location moves toward the leading edge as the initial disturbance amplitudes increase. For a sample application, the simulation data were used to confirm a proposed theoretical model for the transition region. The results from the three simulations collapsed onto the single weighting factor, which characterizes the transition model, and, thus, validates the correlation.

The results are documented for use with future amplitude-based transition–prediction models and for the verification of future theories that model the initial region of transition.

References

[1]Collier, F. S., Jr., private communication, NASA Langley Research Center, 1993.

[2]Manuel, G. S., and Doty, W. A., "A Flight Test Investigation of Certification Requirements for Laminar-Flow General Aviation Airplanes," AIAA Paper 90-1310, May 1990.

[3]Maddalon, D. V., Collier, F. S., Jr., Montoya, L. C., and Land, C. K., "Transition Flight Experiments on a Swept Wing with Suction," AIAA Paper 89-1893, June 1989.

[4]Gaster, M., "A Simple Device for Preventing Turbulent Contamination on Swept Leading Edges," *Journal of the Royal Aeronautical Society*, Vol. 69, Nov. 1965, pp. 788, 789.

[5]Arnal, D., Coustols, E., and Juillen, J. C., "Experimental and Theoretical Study of Transition Phenomena on an Infinite Swept Wing," *Laminar-Turbulent Transition*, edited by V. V. Kozlov, Springer–Verlag, Berlin, 1984, pp. 553–561.

[6]Poll, D. I. A., "Some Observations of the Transition Process on the Windward Face of a Long Yawed Cylinder," *Journal of Fluid Mechanics*, Vol. 150, Jan. 1985, pp. 329–356.

[7]Bippes, H., and Nitschke-Kowsky, P., "Experimental Study of Instability Modes in a Three-Dimensional Boundary Layer," AIAA Paper 87-1336, June 1987.

[8]Müller, B., and Bippes, H., "Experimental Study of Instability Modes in a Three-Dimensional Boundary Layer," AGARD-CP-438, Oct. 1988.

[9]Dagenhart, J. R., Saric, W. S., Mousseux, M. C., and Stack, J. P., "Crossflow-Vortex Instability and Transition on a 45-Degree Swept Wing," AIAA Paper 89-1892, June 1989.

[10]Dagenhart, J. R., and Saric, W. S., "Crossflow Stability and Transition Experiments in a Swept-Wing Flow," NASA TP, 1994.

[11]Dallman, U., and Bieler, H., "Analysis and Simplified Prediction of Primary Instability of Three-Dimensional Boundary-Layer Flows," AIAA Paper 87-1337, June 1987.

[12]Fischer, T. M., and Dallmann, U., "Primary and Secondary Stability Analysis Applied to the DFVLR-Transition Swept-Plate Experiment," AGARD-CP-438, Oct. 1988.

[13]Choudhari, M., "Roughness-Induced Generation of Crossflow Vortices in Three-Dimensional Boundary Layers," *Theoretical and Computational Fluid Dynamics*, Vol. 6, No. 1, 1994, pp. 1–30.

[14]Crouch, J. D., "Receptivity of Three-Dimensional Boundary Layers," AIAA Paper 93-0074, Jan. 1993.

[15]Joslin, R. D., and Streett, C. L., "The Role of Stationary Crossflow Vortices in Boundary-Layer Transition on Swept Wings," *Physics of Fluids A*, Vol. 6, No. 10, 1994, p. 3442.

[16]Lin, R.-S., and Reed, H. L., "Navier–Stokes Simulation of Stationary Crossflow Vortices on a Swept Wing," *Bulletin of the American Physical Society*, Vol. 36, No. 10, 1991, p. 2631.

[17]Fuciarelli, D. A., and Reed, H. L., "Stationary Crossflow Vortices," *Physics of Fluids A*, Vol. 4, No. 9, 1992, p. 1880.

[18]Cooke, J. C., "The Boundary Layer of a Class of Infinite Yawed Cylinders," *Proceedings of the Cambridge Philosophical Society*, Vol. 46, Pt. 1, 1950, p. 645.

[19]Falkner, V. M., and Skan, S. W., "Some Approximate Solutions of the Boundary-Layer Equations," *Philosophical Magazine*, Vol. 12, Nov. 1931, p. 865.

[20]Joslin, R. D., Streett, C. L., and Chang, C.-L., "Validation of Three-Dimensional Incompressible Spatial Direct Numerical Simulation Code—A Comparison with Linear Stability and Parabolic Stability Equations Theories for Boundary-Layer Transition on a Flat Plate," NASA TP-3205, 1992.

[21]Joslin, R. D., Streett, C. L., and Chang, C.-L., "Spatial Direct Numerical Simulation of Boundary-Layer Transition Mechanisms: Validation of PSE Theory," *Theoretical and Computational Fluid Dynamics*, Vol. 4, No. 6, 1993, pp. 271–288.

[22]Williamson, J. H., "Low-Storage Runge–Kutta Schemes," *Journal of Computational Physics*, Vol. 35, No. 1, 1980, pp. 48–56.

[23]Streett, C. L., and Hussaini, M. Y., "A Numerical Simulation of the Appearance of Chaos in Finite-Length Taylor-Couette Flow," *Applied Numerical Mathematics*, Vol. 7, No. 1, 1991, pp. 41–71.

[24]Danabasoglu, G. Biringen, S., and Streett, C. L., "Spatial Simulation of Instability Control by Periodic Suction and Blowing," *Physics of Fluids A*, Vol. 3, No. 9, 1991, pp. 2138–2147.

[25]Streett, C. L., and Macaraeg, M. G., "Spectral Multi-Domain for Large-Scale Fluid Dynamic Simulations," *Applied Numerical Mathematics*, Vol. 6, No. 1–2, 1989/1990, pp. 123–140.

[26]Kachanov, Y. S., and Tararykin, O. I., "The Experimental Investigation of Stability and Receptivity of a Swept-WingFlow," *Laminar-Turbulent Transition*, edited by D. Arnal and R. Michel, Springer–Verlag, Berlin, 1990, pp. 499–503.

[27]Kohama, Y., Saric, W. S., and Hoos, J. A., "A High Frequency, Secondary Instability of Crossflow Vortices that Leads to Transition," *Bulletin of the American Physical Society*, Vol. 35, No. 10, 1990, p. 2331.

[28]Reed, H. L., and Fuciarelli, D. A., "High Frequency Breakdown in Swept-Wing Flows," *Bulletin of the American Physical Society*, Vol. 36, No. 10, 1991, p. 2630.

[29]Balachandar, S., Streett, C. L., and Malik, M. R., "Secondary Instability in Rotating Disk Flow," AIAA Paper 90-1527, June 1990.